Proceedings 10th NUMGE 2023
10th European Conference on Numerical Methods in Geotechnical Engineering
Zdravkovic L, Kontoe S, Taborda DMG, Tsiampousi A (eds)

https://doi.org/10.53243/NUMGE2023-269

FEniCS simulation of a partially saturated slope under varying environmental loads

A. Abed[1], E. Gerolymatou[2], M. Karstunen[1]

[1]*Architecture and Civil Engineering, Chalmers University of Technology, Gothenburg, Sweden*
[2]*Technical University of Clausthal, Clausthal-Zellerfeld, Germany*

ABSTRACT: This paper presents a numerical simulation of the response of a partially saturated slope under the impact of a long heavy rainfall event. The results are shown as a chart of varying safety factor over time. The powerful FEniCS finite element framework is employed to solve the governing coupled Hydro-Mechanical (HM) balance equations. An extended version of the Mohr-Coulomb failure criterion that accounts for partial saturation is implemented in Fortran and called from within FEniCS script to carry out the stress integration and plastic correction. The safety calculations are performed using the strength reduction technique, firstly using Bishop's effective stress, and secondly using two independent stress measures (i.e., net stress and suction). The impact of the chosen stress measures on the results is briefly discussed. The results highlight the importance of considering the unsaturated soil behaviour in the estimation of the safety margin, and to answer the important question of when and where the failure might occur.

Keywords: Slope stability, FEM, FEniCS, Unsaturated soil, Coupling.

1 INTRODUCTION

There is an increasing global awareness of the effect of changing climate on the stability of existing geostructures. The increasing temperature and temperature fluctuations lead to increasing extreme environmental loads and scenarios that should be accounted for when designing and/or checking the stability of slopes.

Increasing rainfall intensity, as well as the longer dry seasons, are just examples of these effects. The changes in the rainfall intensity have a direct consequence, in particular for the marginally stable natural slopes. Typically, such slopes are steep, silty, and most likely only stable due to the contribution of negative pore water pressure (matric suction). Thus, understanding the effect of the unsaturated zone and the variation of suction due to varying rainfall is crucial for a valid prediction of the stability of natural slopes.

The solution of this type of problems, however, needs a comprehensive framework that bases on the mechanics of partially saturated soils and considers the interaction (coupling) between the mechanical processes and the associated hydraulic processes. That usually results in a set of hydro-mechanically coupled set of partial differential equations that need to be solved with advanced numerical tools, such as the Finite Element Method (FEM), as adopted is this paper.

During the last 40 years, there has been a lot of advances in this area, resulting in well-established software that can be used to solve the coupled hydro-mechanical problems (for details see e.g. Abed and Sołowski, 2017). Nonetheless, most of these codes are either commercial, or even when freely available, not open source which poses a challenge in case one needs to adjust or improve some feature to address the user's need.

To tackle this problem, FEniCS (Logg et al., 2012), an open-source framework for solving partial differential equations using the FEM, is used in this paper to show one of the countless possibilities to benefit from this framework to solve the coupled partial differential equations that are derived to describe the hydro-mechanical behaviour of partially saturated soil. The paper details how to use the framework to evaluate the stability of partially saturated slopes under varying precipitation.

2 GOVERNING BALANCE EQUATIONS

The addressed problem involves solving the mechanical balance equation coupled to the mass balance of the liquid component, which is water in the case of a natural slope. In more comprehensive analysis, the solution should also include the mass balance of any gaseous components (dry air, water vapour etc.), the energy balance for thermal flow calculations and mass balance for chemicals and so on, depending on the complexity of the problem (Abed and Sołowski, 2017). For common

geotechnical application, such as the problem treated, the involved gas is typically air, which is usually assumed to stay at the reference atmospheric pressure and thus can be set to zero and neglected in the solution.

In this paper, the problem is considered isothermal, and no chemicals are included in the solution here. These assumptions lead to the following balance equations to solve.

2.1 Mechanical balance equation

The static mechanical balance equation is written as:

$$\nabla \cdot \boldsymbol{\sigma} + \boldsymbol{b} = 0 \qquad (1)$$

where $\nabla \cdot \boldsymbol{\sigma}$ is the divergence of the total stress tensor and $\mathbf{b}$ is a vector containing the body forces.

The geotechnical community agrees that there are basically two methods to represent the stresses in the partially saturated region:

a) based on the Bishop's effective stress $\boldsymbol{\sigma}' = \boldsymbol{\sigma}'' + \chi \boldsymbol{s}$ where $\boldsymbol{\sigma}'' = \boldsymbol{\sigma} - \boldsymbol{u_a}$ is the net stress, $\boldsymbol{s} = \boldsymbol{u_a} - \boldsymbol{u_w}$ is the matric suction and χ is a saturation-dependent, and hence material dependent, coefficient which varies between 0 for dry soil and 1 for fully saturated state. The symbols $\boldsymbol{u_a}$ and $\boldsymbol{u_w}$ denote the pore air pressure and the pore water pressure, respectively.

b) use two independent stress measures, namely the net stress $\boldsymbol{\sigma}''$ and matric suction $\boldsymbol{s}$ (among several other possible compinations) (Gens et al., 2006).

While the first option is more appealing from a numerical point of view, there is still no general agreement on the value of the factor χ to be used. There is also some criticism on the validity of using such a ¨constitutive parameter¨ that is material dependent in a stress measure (Fredlund and Rahardjo, 1993). Nevertheless, it seems that the most accepted value (Gens et al., 2006), and hence the one used in this paper, is $\chi = S_{eff}$ where S_{eff} is the so-called effective degree of saturation being defined as $S_{eff} = (S_r - S_{res})/(S_{sat} - S_{res})$ with S_r, S_{sat} and S_{res} denoting the soil degree of satuation at normal conditions, the degree of saturation at full saturation and the residual degree of saturation, respectively. As a consequence, the definition of Bishop's effective stress requires information from the Soil Water Characteristic Curve, SWCC.

On the other hand, the independent stress measures do not require such ¨constitutive¨ assumptions and are thus more robust in satisfaying the continuum mechanics requirements for the definition of stress measures. However, there are some numerical drawbacks during the transition from unsaturated to fully saturated state, where one should be careful to recover the single Terzaghi's effective stress measure $\boldsymbol{\sigma}' = \boldsymbol{\sigma} - \boldsymbol{u_w}$ by setting suction $\boldsymbol{s} = \mathbf{0}$ which yields that $\boldsymbol{u_a} = \boldsymbol{u_w}$ and the net stress $\boldsymbol{\sigma}'' = \boldsymbol{\sigma}' = \boldsymbol{\sigma} - \boldsymbol{u_w}$.

Based on which option one chooses the weak formulation of Equation (1) becomes:

for single Bishop's effective stress measure:

$$\int_\Omega \nabla N_b^T \boldsymbol{M} \nabla N_b \delta\hat{u}\, \mathrm{d}\Omega + \int_\Omega \chi \nabla N_b^T \boldsymbol{m^T} \nabla N_b \delta\widehat{u_w}\, \mathrm{d}\Omega - \int_\Omega N_b \delta b\, \mathrm{d}\Omega - \int_\Gamma N_b \delta t\, \mathrm{d}\Gamma = 0 \qquad (2)$$

for two independent stress measures:

$$\int_\Omega \nabla N_b^T \boldsymbol{M} \nabla N_b \delta\hat{u}\, \mathrm{d}\Omega + \int_\Omega \nabla N_b^T \boldsymbol{m^T} \nabla N_b \delta\widehat{u_a}\, \mathrm{d}\Omega - \int_\Omega N_b \delta b\, \mathrm{d}\Omega - \int_\Gamma N_b \delta t\, \mathrm{d}\Gamma = 0 \qquad (3)$$

where N_b , $\delta\hat{u}$, $\delta\widehat{u_w}$, $\delta\widehat{u_a}$ and δt are the shape function, the increment of displacements, the increment of pore water pressure, the increment of pore air pressure and the surface traction increment, respectively. In most common cases the pore air pressure is considered to stay atmospheric with $u_a = 0$, and thus the second term in Equation (3) disappears. The symbol $\boldsymbol{m^T}$ denotes the transpose of the unity vector and $\mathbf{M}$ represents the material stiffness matrix. In fact, the term $\int_\Omega \nabla N_b^T \boldsymbol{M} \nabla N_b \delta\hat{u}\, \mathrm{d}\Omega = \int_\Omega \nabla N_b^T \delta\boldsymbol{\sigma}'\, \mathrm{d}\Omega$ which shows that a suitable procedure should be employed for stress integration during the solution advancement. The integration could be implicit or explicit and heavily dependent on the stress-strain relationship used to model the material. To achieve the required accuracy in FEM this integration should be carried out at specific locations within the finite element known as the stress integration points. Given the focus on the soil stability, without caring too much about the pre-failure deformations, the well-known Mohr-Coulomb (MC) model is thought to be enough for the purposes of this study.

2.2 Water mass balance equation

The water mass balance equation for unsaturated soil can be written as (Abed and Sołowski, 2017):

$$\nabla^T \left[\frac{\mathrm{K}(s)}{\rho_w g} \cdot (\nabla u_w + \rho_w g)\right] + \mathrm{n}\left(\frac{\partial S_r}{\partial s} - \frac{S_r}{K_w}\right)\frac{\partial u_w}{\partial t} + S_r \frac{\partial \varepsilon_v}{\partial t} = 0 \qquad (4)$$

where n, ρ_w, g and K_w are the porosity, density of water, the gravity acceleration, and the water bulk modulus, respectively. Note that for unsaturated soils, the hydraulic conductivity is no longer constant, but a function of the suction s. Also the derivative of the degree of saturation with respect to suction appears in the equation. As a consequence, both the SWCC and the hydraulic conductivity function need to be defined before starting the analysis. The term $S_r \frac{\partial \varepsilon_v}{\partial t}$ reflects the effect of volumetric strain rate due to mechanical

deformation $\frac{\partial \varepsilon_v}{\partial t}$ on the water balance equation and thus it is the Hydro-Mechanical coupling term in Equation (4). The corresponding weak formulation of the water balance equation reads as follows:

$$-\int_\Omega \nabla N_b^T \frac{\mathrm{K}(s)}{\rho_w g} \nabla N_b \widehat{u_w} \mathrm{d}\Omega + \int_\Omega \nabla N_b^T \frac{\mathrm{K}(s)}{\rho_w g} \rho_w g \, \mathrm{d}\Omega + \int_\Omega N_b \, \mathrm{n} \left(\frac{\partial S_r}{\partial s} - \frac{S_r}{K_w}\right) \frac{d\widehat{u_w}}{dt} \mathrm{d}\Omega + \int_\Omega N_b \, S_r \frac{\partial \varepsilon_v}{\partial t} \, \mathrm{d}\Omega = 0 \quad (5)$$

3 MOHR-COULOMB MODEL FOR UNSATURATED SOIL

Depending on the stress measure(s) used, the mathematical formulation of the MC model differs slightly. Upon using the single Bishop's effective stress measure, the model can be applied in the standard form where:

$$f_M = \left(\frac{\sigma_1' - \sigma_3'}{2}\right) - \left(\frac{\sigma_1' + \sigma_3'}{2}\right) \cdot \sin\varphi' - c' \cdot \cos\varphi' \quad (6)$$

$$g_M = \left(\frac{\sigma_1' - \sigma_3'}{2}\right) - \left(\frac{\sigma_1' + \sigma_3'}{2}\right) \cdot \sin\psi \quad (7)$$

$$f_T = g_T = \sigma^t - \sigma_3' \quad (8)$$

with compression considered positive. The symbols f_M and g_M denote the failure and the plastic potential surface, respectively. The model includes an additional tension cutoff failure surface indicated by f_T. To describe the plastic behaviour, the model requires input of the shear strength parameters, namely the effective internal friction angle φ', the effective cohesion intercept c' and the dilatancy angle ψ. On top of that, the tensile strength σ^t should be provided, which is most often set to zero by default. The classical Hooke's linear elasticity law is followed during elasticity which requires only two elastic material properties, the effective Young's modulus E' and the effective Poisson's ratio υ'.

In the case of two independent stress measures, the model is written as:

$$f_M = \left(\frac{\sigma_1'' - \sigma_3''}{2}\right) - \left(\frac{\sigma_1'' + \sigma_3''}{2}\right) \cdot \sin\varphi' - c \cdot \cos\varphi' \quad (9)$$

$$g_M = \left(\frac{\sigma_1'' - \sigma_3''}{2}\right) - \left(\frac{\sigma_1'' + \sigma_3''}{2}\right) \cdot \sin\psi \quad (10)$$

$$f_T = g_T = \sigma^t - \sigma_3'' \quad (11)$$

where the total cohesion c includes the contribution of suction in form of capillary cohesion, as well as the effective cohesion intercept, and is expressed as:

$$c = c' + \underbrace{s \cdot S_{eff} \cdot \tan\varphi'}_{capillary\ cohesion} \quad (12)$$

The assumed capillary cohesion relies on Vanapalli et al., (1996) for experimentally supported conclusions.

The elastic part of the model follows a slightly modified linear elasticity formulation to enable suction effects:

$$\Delta\boldsymbol{\varepsilon}^e = \Delta\boldsymbol{\varepsilon}_\sigma^e + \boldsymbol{m}^T \Delta\boldsymbol{\varepsilon}_s^e;\ \Delta\boldsymbol{\varepsilon}_s^e = \frac{\Delta s}{H_s} \quad (13)$$

where the elastic strain increment $\Delta\boldsymbol{\varepsilon}^e$ has two components in this case, one due to net stress increment $\Delta\boldsymbol{\varepsilon}_\sigma^e$ and one due to suction increment $\Delta\boldsymbol{\varepsilon}_s^e$. The elastic suction strain increment is controlled by the suction dependent elastic modulus $H_s = 3K_s$ where K_s is the soil bulk modulus with respect to suction which can be measured experimentally. It is worthy to mention that during mechanical calculations $\Delta\boldsymbol{\varepsilon}_s^e$ is imposed and not an output of FE mechanical calculations, as H_s is given and Δs is calculated from the water balance equation.

4 NUMERICAL IMPLEMENTATION

FEniCS allows for a relatively straight forward implementation and coupling of the balance equations (1) and (4). The stress integration routines of the two versions of Mohr-Coulomb model consistent with Bishop's effective stress and the two independent stress measures are implemented using Fortran based on the method proposed by De Borst, (1987). A special routine was developed to link Fortran routines to the Python script used to communicate with FEniCS in a way similar to Stefanou (2018). This enables much faster calculations during stress integration if compared to the direct implementation of the stress integration routines in Python. Another thing which is crucial for the speed of calculations is the use of the special 'Quadrature' element in FEniCS that allows for the iterative global finite element calculations to be performed at the stress integration point, and thus preserving the quadratic rate of convergence, provided that the correct consistent tangent operator is fed to FEniCS (Logg et al., 2012).

5 VERIFICATION BENCHMARK

To verify the implementation, a simple 2D plane strain problem is solved using the developed Python script for FEniCS and compared to the results of GeoStudio, a well-established commercial software for geotechnical calculations that allows for unsaturated soil behaviour to be considered.

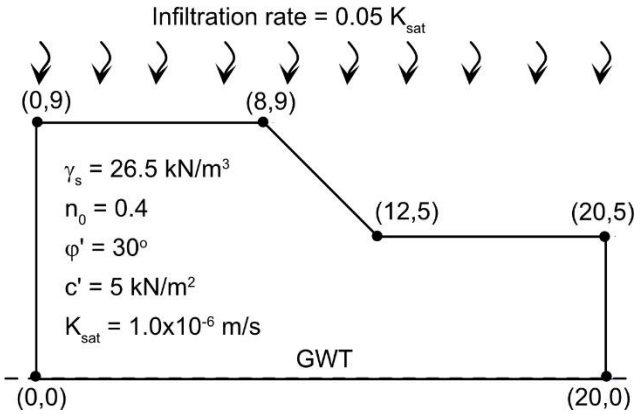

Figure 1. Slope geometry, soil properties and infiltration rate.

Table 1. Slope soil properties

property	value	unit
$\boldsymbol{\varphi'}$	30	[°]
$\boldsymbol{c'}$	5	kN/m^2
$\boldsymbol{\psi}$	0	[°]
$\boldsymbol{\gamma_s}$	26.5	kN/m^3
$\boldsymbol{E'}$	24000	kN/m^2
$\boldsymbol{H_s}$	100000	kN/m^2
$\boldsymbol{v'}$	0.2	[o]
$\boldsymbol{\sigma^t}$	0	kN/m^2
$\boldsymbol{K_{sat}}$	1×10^{-6}	m/s
$\boldsymbol{\alpha}$	0.02	1/kPa
$\boldsymbol{n_o}$	0.4	[-]

5.1 Finite element model

Figure 1 shows the geometry of the modelled slope. The assigned material properties are listed in Table 1.

The groundwater table is assumed to be at 9 m below the slope surface with an initial hydrostatic suction distribution above it.

The used finite element mesh, which can be seen in Figure 3, is generated using Gmsh and then imported to FEniCS.

After applying a gravity loading in the first calculation stage, the slope is subjected to an extreme lengthy rainfall event which lasts for 30 days with a constant infiltration rate of 0.05K_{sat}. The main idea here is just to test the response of the model and how the suction variation would affect the stability of the slope, regardless how much the scenario is realistic or not. The strength reduction technique is also implemented in the Python script used to communicate with FEniCS to estimate the safety factor evolution during the rainfall event. According to this technique, the HM coupling is frozen by forcing an extremely small time step and the shear strength parameters are reduced progressively until failure happens. The ratio between the available shear strength parameters to the critical ones needed to cause failure gives the safety factor FS:

$$FS = \frac{c'}{c'_{critical}} = \frac{\tan\varphi'}{\tan\varphi'_{critical}} \qquad (14)$$

Note that in the case when the two independent stress variables are used, the strength reduction will affect the capillary cohesion defined in Equation (12) through the reduction of φ'. The numerical divergence during the equilibrium calculation is used as a criterion to indicate numerical failure, and thus physical failure needs to be supported by the visual inspection of the creation of a fully developed failure mechanism in the output. The failure is deemed to happen if the calculation does not converge within 500 iterations (Huang and Griffiths, 2008).

For the unsaturated water flow, the SWCC is given as:

$$S_r = (S_{sat} - S_{res}) \cdot e^{-\alpha \cdot s} + S_{res} \qquad (15)$$

where α is a material parameter. The corresponding hydraulic conductivity function is described by the equation:

$$K(s) = K_{sat} \cdot e^{-\alpha \cdot s} \qquad (16)$$

These functions are chosen for simplicity. However, the framework is very flexible in the sense that any SWCC and hydraulic conductivity function can be easily implemented and incorporated into the code.

The soil unit weight γ is updated based on the saturation where $\gamma = (1-n)\,\gamma_s + S_r n \gamma_w$ with γ_s and γ_w denoting the unit weight of the soil solid particle and water, respectively.

FEniCS offers the possibility to write the calculation's output in multiple formats. For this study, Paraview is used as the tool to investigate the results.

5.2 Numerical results and discussion

Figure 2 shows the calculated evolution of safety factor during the rainfall event, one based on Bishop's effective stresses and another based on the two independent stress measures assumption. Both methods resulted in a monotonic reduction in safety factor due to suction loss because of continuous infiltration. However interestingly, at least for the calculated example, the two independent stress measures prediction is more conservative, as an initial SF = 1.92 under initial hydrostatic suction distribution was predicted which kept reducing with infiltration until it reached 1.62 at the end of the rainfall event compared to an initial SF = 2.4 and final SF = 2.05 predicted by the calculations based on Bishop's effective stress. By investigating the failure mechanism in both cases, the calculations based on Bishop's effective stress always resulted in a well-defined, relatively shallow, failure mechanism, see Figure 3, whereas the failure mechanism is more deep and not well-formed in the case of two independent stress measures, see Figure 4.

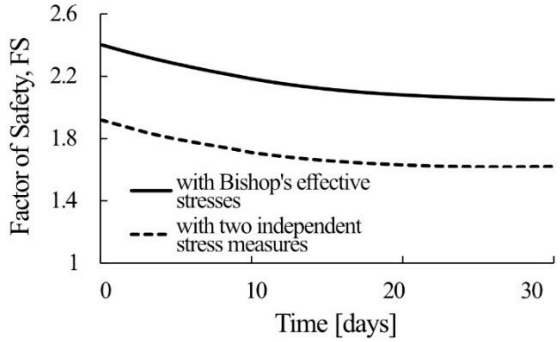

Figure 2. Calculated safety factor over time using Bishop's effective stress and using two independent stress measures.

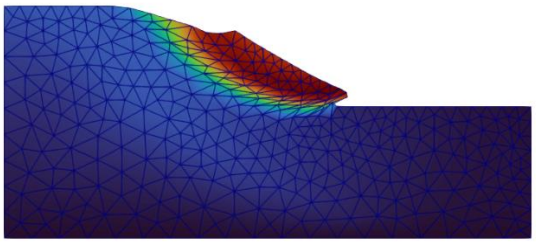

Figure 3. Deformed mesh after strength reduction at the end of the 30 days rainfall event using Bishop's effective stresses.

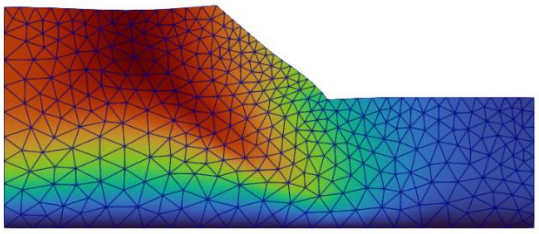

Figure 4. Deformed mesh after strength reduction at the end of the 30 days rainfall event using two independent stress measures.

That might be related to the spatial variation in total cohesion value with degree of saturation in the latter.

5.2.1 FEniCS versus GeoStudio results

Geostudio was used to simulate the same problem. The module Seep/W uses the finite element method to calculate the pore water pressure distribution over time, and Slope/W uses the limit equilibrium method (LEM) to estimate the safety factor at the required time step. For LEM calculations, Morgenstern-Price method is employed with Mohr-Coulomb failure criterion extended to include partial saturation effects on shear strength. The GeoStudio calculations are considered uncoupled when compared to the method developed in this paper.

Figure 5 shows the failure mechanism as predicted by FEniCS calculations using Bishop's stress which compares very well to the critical slip surface estimated by GeoStudio as presented in Figure 6. However, Geostudio yielded a slightly higher safety factor of 2.26 after 30 days of rainfall.

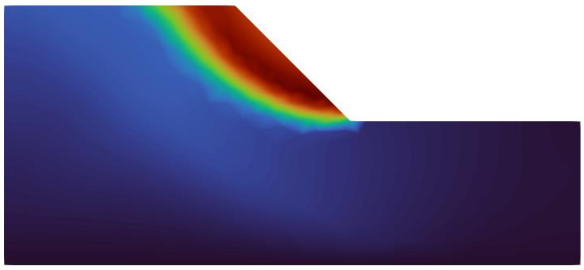

Figure 5. Predicted failure mechanism in terms of total displacements after strength reduction at the end of the 30 days rainfall event using Bishop's effective stresses. The predicted Safety Factor is 2.05.

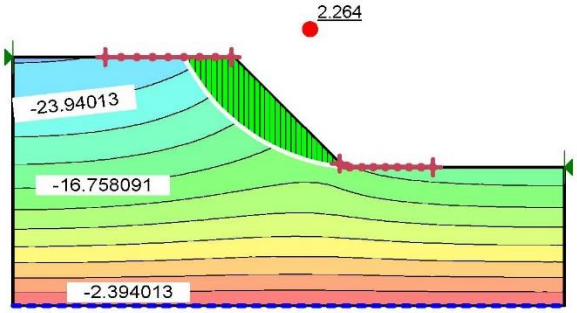

Figure 6. The critical slip surface, the calculated Safety Factor and pore water pressure distribution after 30 days of the rainfall event as calculated by Geostudio.

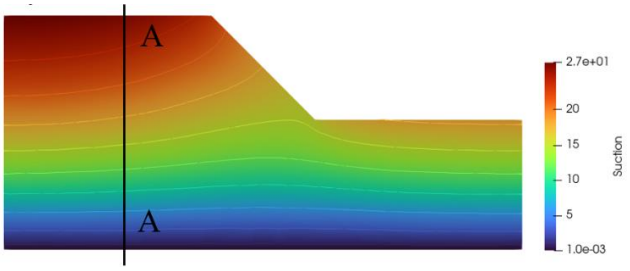

Figure 7. Pore water pressure distribution after 30 days of the rainfall event as calculated using FEniCS.

Figure 6 also presents the contours of suction distribution after 30 days of infiltration, which perfectly match the FEniCS calculations shown in Figure 7.

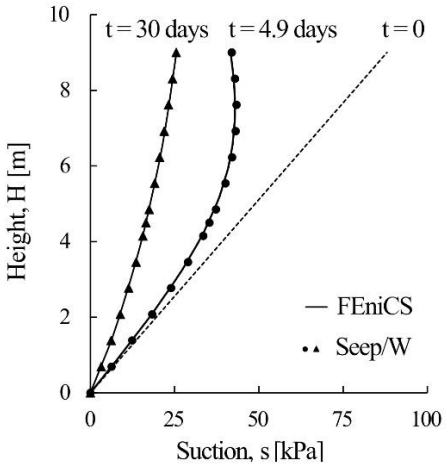

Figure 8. Pore water pressure at section A-A after 4.9 and 30 days of infiltration as calculated using FEniCS and Seep/W.

To verify the results more, the suction profile along the section A-A in Figure 7 after 4.9 and 30 days as calculated using FEniCS, is compared in Figure 8 to Seep/W calculations. The perfect match verifies the code implementation used in FEniCS calculations. The perfect match also indicates that the coupling effects are negligible in this case.

6 3D SLOPE STABILITY CALCULATIONS

The FEniCS framework makes it extremely flexible once one gets the 2D version functional to move directly to 3D space or vice versa. It takes only little effort to change the dimensions of some vectors in the Python script and, of course, generating a suitable 3D mesh to start getting the required results. All of that assuming that the implementation of the constitutive material model is also compatible with 3D calculations.

As an example, a 3D counterpart slope to the 2D one solved above was subjected to similar mechanical, hydraulic boundary conditions and calculation stages including the strength reduction. Figure 9 presents the predicted failure mechanism resulting from the strength reduction stage after 30 days of water precipitation. The predicted safety factor in this case is FS = 2.3 compared to 2.05 in the 2D version which is expected due to the 3D effects known to increase the safety factor and a coarser mesh.

7 CONCLUSIONS

The first two authors developed a Python code which can communicate with FEniCS to carry out a fully coupled hydro-mechanical analysis for the response of unsaturated soils. The code is also able to read Fortran libraries that contains stress integration routine, or any other type of useful functions, to increase the speed of calculations.

This paper presented an example of such possible analyses focussing on the stability calculations of a partially saturated slope subjected to varying environmental loads. In addition to the fully coupled deformation analysis the code is able to perform strength reduction analysis using either Bishop's effective stress or two independent stress measures namely, net stress and matric suction.

The slope stability calculations showed that no matter which stress measure one uses, the safety factor tends to reduce with reducing suction, however, at least for the discussed example, the calculations based on the two independent stress measures tend to produce more conservative values with less defined failure surface. This conclusion is still very premature and needs much more investigations to be generalized. Furthermore, implementation was satisfactorily verified against the results from Geostudio. The possibility to do full 3D stability calculations was furthermore demonstrated, with reasonable results. Finally, the code forms a corner stone for further developments to benefit from the powerful capabilities of FEniCS framework and employ it to solve the challenging geotechnical problems.

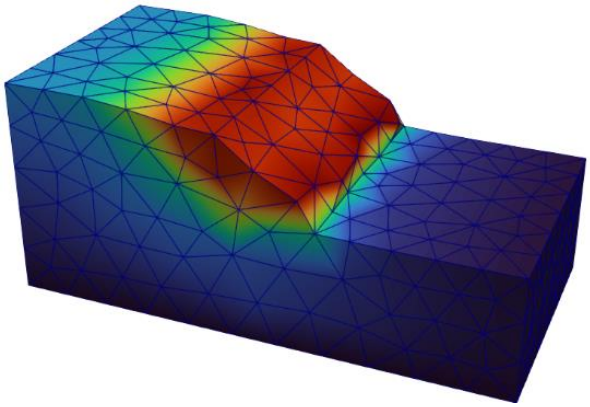

Figure 9. 3D failure mechanism after 30 days of infiltration. The predicted safety factor is 2.3 using Bishop's stresses.

8 ACKNOWLEDGEMENTS

The work is funded by Formas (Research Council for sustainable Development, Grant (2021-02400) and Swedish Transport Administration (Grant 2022/69758) via BIG (Better Interaction in Geotechnics.The work is done as part of Digital Twin Cities Centre that is supported by Sweden's Innovation Agency VINNOVA (Grant 2019-00041).

9 REFERENCES

Abed, A., Sołowski, W., 2017. A study on how to couple thermo-hydro-mechanical behaviour of unsaturated soils: Physical equations, numerical implementation and examples. Comput. Geotech. 92, 132–155.

De Borst, R., 1987. Integration of plasticity equations for singular yield functions. Comput. Struct. 26, 823–829.

Fredlund, D.G., Rahardjo, H., 1993. Soil mechanics for unsaturated soils. John Wiley & Sons.

Gens, A., Sánchez, M., Sheng, D., 2006. On constitutive modelling of unsaturated soils. Acta Geotech. 1, 137–137.

Huang, J., Griffiths, D.V., 2008. Observations on return mapping algorithms for piecewise linear yield criteria. Int. J. Geomech. 8, 253–265.

Logg, A., Mardal, K.-A., Wells, G., 2012. Automated solution of differential equations by the finite element method: The FEniCS book. Springer Science & Business Media.

Stefanou, I., 2018. "Numerical Geolab", Controlling earthQuakes project. Nantes. url: www.coquake.eu.

Vanapalli, S.K., Fredlund, D.G., Pufahl, D.E., Clifton, A.W., 1996. Model for the prediction of shear strength with respect to soil suction. Can. Geotech. J. 33, 379–392.